MICROCOPY RESOLUTION TEST CHART
NATIONAL BUREAU OF STANDARDS-1963-A

FTD-ID(RS)T-0245-82

FOREIGN TECHNOLOGY DIVISION

LASER JOURNAL

(Selected Articles)

84   07   10   140

FTD-ID(RS)T-0245-82

EDITED TRANSLATION

FTD-ID(RS)T-0245-82   26 May 1982

MICROFICHE NR: FTD-82-C-000698

LASER JOURNAL (Selected Articles)

English pages: 32

Source: Laser Journal, Vol. 6, Nr. 9, September 1979,
         pp. 5-10; 31-38
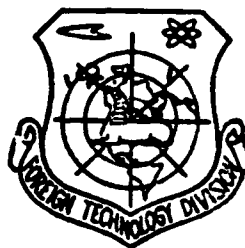
Country of origin: China
Translated by: LEO KANNER ASSOCIATES
                F33657-81-D-0264
Requester: FTD/TQTD
Approved for public release; distribution unlimited.

FTD -ID(RS)T-0245-82   Date 26 May 19 82

Table of Contents

GRAPHICS DISCLAIMER

All figures, graphics, tables, equations, etc. merged
into this translation were extracted from the best
quality copy available.

ANALYSIS OF OUTPUT PULSE PROFILES OF A TEA CO_2 LASER

Lou Chihong, Yu Shusheng, and Ding Aizhen
Shanghai Institute of Optics and Fine Mechanics, Chinese Academy of Sciences
Submitted 12 January 1979

The output characteristics of a TEA CO_2 laser for various
gas mixtures and various pump levels are quantitatively calculated
using time-varying electron excitation coefficients. The calcula-
tion results are in good agreement with those of experiments.
According to the theory of partial population inversion suggested
by Polanyi, the conditions for partial population of CO_2 molecules
are discussed. The single peak of the output pulse for gas mix-
tures involving N_2 is explained with the partial population inver-
sion.

Since Beaulieu's [1] first report on the TEA CO_2 laser in 1970, this laser
type has become a valuable aid in laser nuclear fusion, isotope isolation, laser
processing, laser radar, and radar chemistry. The output pulse profile of TEA
CO_2 laser generally consists of an 100-nanosecond increment-switch pulse with an
1 to 2 milliseconds tail. The authors used a photon traction examining and
measuring device to investigate the pulse profiles of ultraviolet pre-ionization
TEA CO_2 laser [2] and observe various waveforms at different pumping levels.
Moreover, the authors adopted five temperature dynamics models devised by Manes
and Seguin [3] to analyze and calculate dynamic process of different conditions
in order to explain the experimental results.

1

In Manes and Seguin's calculations, the electron excitation coefficients of various vibration energy levels of CO_2 and N_2 are assumed as constants. Actually, according to the potential waveform (Fig. 1(a)) measured by the authors with non-inductive resistance for partial voltage, the electric field intensity in the discharge process varies with time; however, the electron excitation rate is a function of field intensity. The authors first adopted the non-Maxwell electron distribution function to calculate the average electron energy level u_r of different field intensities and different gas ratios. Then, according to Judd's [4] results to calculate the electron excitation coefficients of different field intensities in order to get time-varying electron excitation coefficients, the experimental situation of the dynamic process can be more effectively revealed by substituting this electron excitation coefficient into the Landau-Taylor equations [3]; this can avoid the randomness in selecting the values of electron excitation coefficients in past calculations.

(a) Potential (peak value is approximately 100 kilovolts).

(b) Current (peak value is approximately 5500 amperes).
Fig. 1. Waveform of electric potential and current (sine wave is used as a time mark).

The Lagrange-Kurd method was used to solve differential equations (refer to appendix) including the laser oscillation equations. The solutions include the stored energy of three CO_2 vibration modes (with the characteristic temperatures, respectively, T_1, T_2 and T_3) and N_2 vibration mode (T_4 as the characteristic temperature), and the variation of laser oscillation intensities with time. The

2

overall calculation time was 2 milliseconds, the initial-step length, $2 \cdot 10^{-9}$ second, the error control quantity, 10^{-4}, and the electron excitation coefficient once for each 0.1 millisecond. This calculation method for the laser output energy can be quantitatively compared with the experimental values; Table 1 lists the results. In the table, the experimental values were obtained with a single-section ultraviolet pre-ionization TEA laser; the laser cavity was composed of a single-section ultraviolet pre-ionization TEA laser; the laser cavity was composed of a total-reflection concave lens and the inherent-characteristic-type germanium plate. The cavity is 2 meters long and the working gas pressure is 600 millimeters of a mercury column. For obtaining relatively stable experiment data within the range of a relatively wider gas ratio, the input energy level is controlled at 100 joules per liter. From Fig. 2, the calculation values are in good agreement with those from the experiments. As an example, Table 1 also lists the calculation values of the average electron energy level u_r while $E/N = 2 \cdot 10^{-16}$ volt·cm^2. Therefore, it can be concluded that the electron excitation coefficient as varying with time can be adopted in calculating the laser output characteristics from the quantitatively surveyed potential and current curves.

Table 1. Laser output characteristics of different gas ratios: * Arc-shaped light appearing locally during discharge.

CO_2 N_2 He			He (%)	(a) u_r (电子伏)	激光输出能量 (b)(焦耳) 实验值	计算值	(e) 效率 (实验值)
8	2	10	67	0.830	17 (c)	15.1 (d)	7%
8	2	8	62	0.762	19	17.5	7.9%
8	2	6	55	0.704	21	20.7	8.7%
8	2	4	44	0.645	25	23.2	10.4%
8	2	3	38	0.610	26.5	28.9	11%
8	2	2	29	0.570	10.4*	32.8	4.3%

* 放电局部出现弧光. 输出下降.

Key: (a) (Electron volt); (b) Laser output energy (joules); (c) Experimental value; (d) Calculation value; (e) Efficiency (experimental value).

Figure 3 presents laser waveform photographs at different pump energies. The authors used the above-mentioned method to calculate waveforms of different pump levels; the calculation results are in good agreement with the experimental

3

results. From the calculation results, at a low pumping level and after the increment switch, the difference between the population of upper-level particles and the population of lower energy-level particles, and those of reverse rotation can be re-established when there is continuous pump action; therefore, a multipeak structure is manifested. At a high pumping level, the difference in populations of upper-level and lower energy-level particles is great and the increment switch has not used up the difference in particle populations and with continuous pump action, a greater tail in the waveform is displayed.
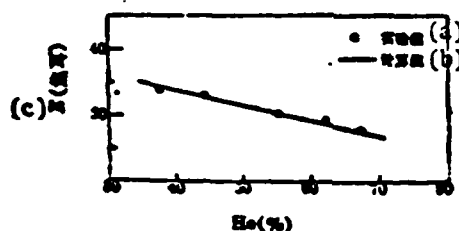

Fig. 2. Laser output, energy of
different gas ratios.
Key: (a) Experimental values;
(b) Calculation values; (c) (Joules).

Generally, the first laser waveform peak is the increment switch pulse; a lower tail is caused by the resonance excitation of N_2-CO_2. When N_2 does not exist, there is no tail as shown in the waveform in Fig. 4(b). However, in the absence of N_2, there is no single-peak waveform with tail as shown in Fig. 4(a). In this case, CO_2:N_2:He=3:2:8. According to the authors' experimental results, the single-peak waveform with tail usually appears when the pumping level is low or when the in-cavity loss is great and the cavity is out of resonance. Therefore, a loss column should be introduced in the laser cavity oscillation equation to replace an item (-ln R) of Manes and Seguin [3] with (2YL-ln R); R is reflectivity, L is cavity length, and Y is loss coefficient. Figure 5 gives the effect of the loss on the laser waveform and the distribution of particle populations. Figure 5(b) shows the result of introducing the loss. In the calculations, R=0.46, L=200, and Y=-0.15 percent/cm. In addition to a large particle population with reverse rotation appearing, in the rear part $N_{001} < N_{100}$ between the vibrational energy level, there is no reverse rotation of the particles with this population. However, the laser still functions between a pair of
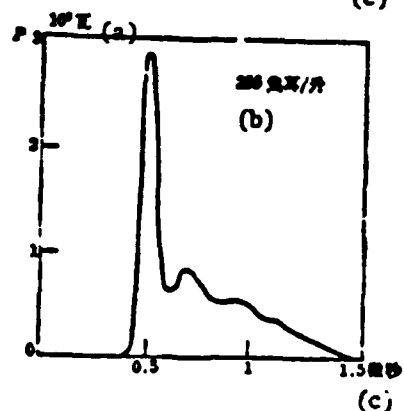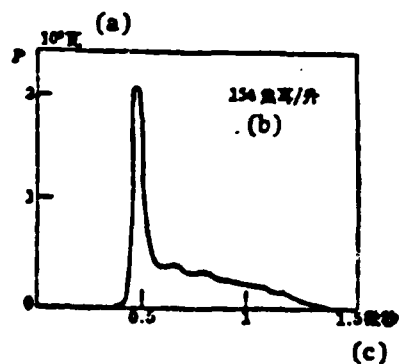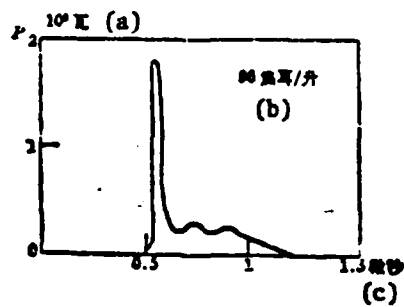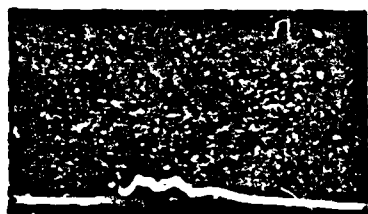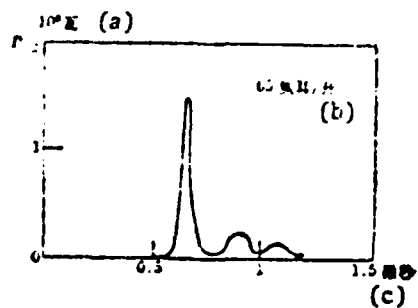
4

Fig. 3. Laser waveforms at different pumping levels (left--experimental photographs; right--computed waveforms).
Key: (a) Watts; (b) Joules/liter; (c) Microseconds.

5

rotational energy levels. This is the case of partial reverse rotation as discussed by Polanyi [5]. In the following, there is an examination of conditions of partial reverse rotation of atoms and molecules.

Let $N_{001,J'}$ represent the quantum number of the N_{001} energy level as the population of particles at the sub-energy level J'; $N_{100,J}$ represent the rotational quantum number at the N_{100} energy level for the population of particles at the sub-energy level J. The condition of reverse rotation of population of particles is $\frac{N_{001,J'}}{2J'+1} > \frac{N_{100,J}}{2J+1}$. If the rotation and temperature of two vibrational energy levels are the same and equal to the gas temperature [6], the reverse-rotation condition is

$$\ln \frac{N_{001}}{N_{100}} > \frac{hc}{kT}[B_{r,001}J'(J'+1)$$

$$- B_{r,100}J(J+1)] + \ln \frac{B_{r,100}}{B_{r,001}} \quad (1)$$

In the equation, $B_{r,001}$ and $B_{r,100}$ are two rotational constants of the energy level; h is Planck's constant, c is the speed of light, and k is Boltzmann's constant. In the dynamic model used in our calculation, the distribution of the population of particles in each vibration mode is subject to Boltzmann's distribution; the characteristic temperatures of the ν_3 and ν_1 vibrational modes of CO_2 are, respectively, T_3 and T_1.

$$N_{001} = \frac{N_{CO_2}}{S_0} \exp(-h\nu_3/kT_3) \quad (2)$$

$$N_{100} = \frac{N_{CO_2}}{S_0} \exp(-h\nu_1/kT_1) \quad (3)$$

$$S_0 = [1 - \exp(-h\nu_1/kT_1)]$$
$$\times [1 - \exp(-h\nu_2/kT_2)]^2$$
$$\times [1 - \exp(-h\nu_3/kT_3)] \quad (4)$$

From equations (2) and (3), we obtain:

$$\ln \frac{N_{001}}{N_{100}} = \frac{h\nu_1}{kT_1} - \frac{h\nu_3}{kT_3} \quad (5)$$

In TEA CO_2 laser, when the input energy is low (less than 200 joules per liter), the temperature rise in the working gas is slight and $T_1 \approx T$. From equations (1) and (5), we can obtain the conditions for partial reverse rotation between the energy levels of three-atom molecule CO_2 laser.

6

(a) CO₂:N₂:He=3:2:9 P=0.4 大气压
输入能量：60 焦耳/立升 (1)
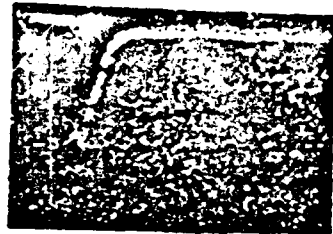
(b) CO₂:He=1:9 P=1 大气压
输入能量：100 焦耳/立升 (2)

(a) 含 N₂ 的单峰波形；(b) 不含 N₂ 的单峰波形
（横坐标：0.5 微秒/格）

Fig. 4. Single-peak-output laser
waveform: (a) single-peak waveform
containing N_2; (b) single-peak wave-
form without N_2 (abscissa: 0.5 micro-
second/lattice).
Key: (1) Atmospheric pressure: input
energy at 100 joules/liter; (2) Atmo-
spheric pressure: input energy at 100
joules/liter.

(1) For Branch P, let $B_r \approx B_{r,001} \approx B_{r,100}$.

$$\frac{h\nu_1}{h\nu_2} < \frac{T}{T_s} < \frac{h\nu_1 + 2JB_r hc}{h\nu_2} \qquad (6)$$

(2) For Branch Q, the difference between $B_{r,001}$ and $B_{r,100}$ cannot te neglected.

$$(B_{r,100} - B_{r,001})J(J+1) > T \ln \frac{B_{r,100}}{B_{r,001}}$$

$$(7)$$

For example, T=300K, requiring J≥23.

7

(3) For Branch B, the partial reverse rotation cannot appear. According to the determinations mentioned above, the authors discovered that in the numerical-simulation calculation of Branch P, only with T_3 satisfying the condition (6), a partial reverse rotation will appear. Table 2 gives the results.

Table 2. Conditions of producing total reverse rotation and partial reverse rotation (Branch P).

反转 (a)	$T=315K$ 时 T_3 允 许 范 围 (b)	T_3 计算值 (c)	N_{011} $\left(\frac{10^{17}}{厘米^3}\right)$	N_{103} $\left(\frac{10^{17}}{厘米^3}\right)$	备 注 (e)
(f) 部分反转	$550K<T_3$ $<560K$	552K	0.3424	0.3533	见图 5(b) (h)
(g) 全反转	$T_3>560K$	576K	0.4422	0.3544	见图 5(a) (i)

Key: (a) Type of reverse rotation; (b) Allowable range of T_3 when T=315K; (c) Computational value of T_3; (d) cm^3; (e) Remarks; (f) Partial reverse rotation; (g) Entirely reverse rotation; (h) Refer to Fig. 5(b); (i) Refer to Fig. 5(a).

From the above table, if an N_2 population exists exhibiting a single-peak waveform with relatively low peak power, this situation applies to the partial reverse rotation of certain particle population in the rear pump period.

In short, the authors adopted the time-varying electron excitation coefficient to quantitatively calculate the laser output energy at different gas ratios; these values are in good agreement with the experimental values. Moreover, the laser output waveforms at different pumping levels are calculated, and the various waveforms observed in experiments are explained. Finally, according to Polanyi's regime of partial reverse rotation, the authors discussed the conditions of partial reverse rotation of the triatomic CO_2 molecule, and explained the single-peak waveform containing N_2. These values are in good agreement with the numerical simulation results produced with a computer.

8
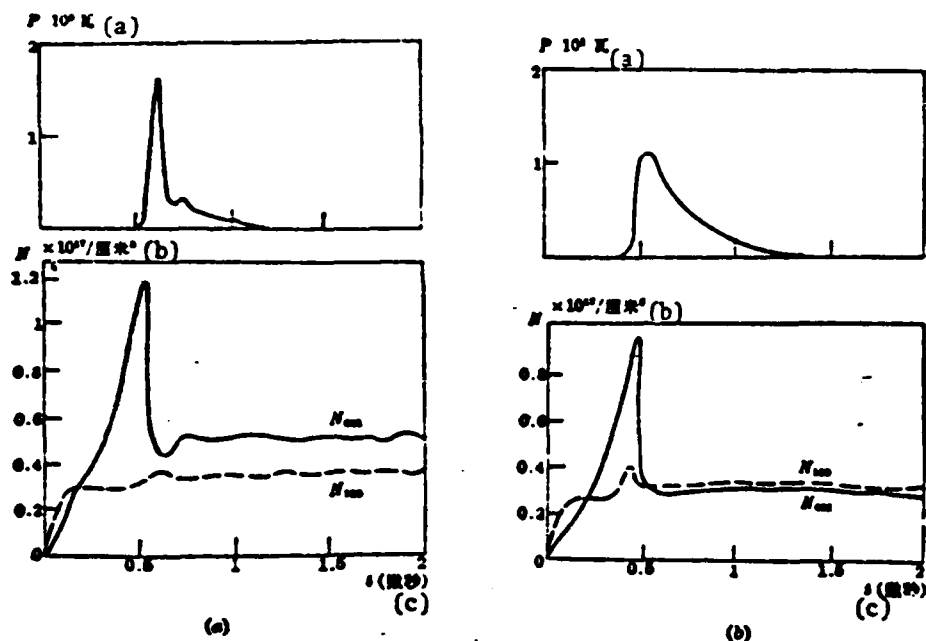
Fig. 5. Variations of laser waveform and distribution of particle popula-
tion with time under two situations: Input energy: 100 joules/liter;
$CO_2:N_2:He=3:2:8$; $P=0.8$ atmospheric pressure; $R=0.46$; $L=2$ meters.
(a) situation of entirely reverse rotation; (b) situation of partial reverse
rotation, assuming $\gamma=0.1$ percent/centimeter.
Key: (a) Watts; (b) cm^3; (c) (Microseconds).

Appendix

Let E_1, E_2, and E_3 represent, respectively, the CO_2 symmetric vibration,
strain vibration, and energy-storing density of the unsymmetrical vibration mode.
E_4 represents the energy-storing density of the N_2 vibration mode (unit at
erg/cm^3).

$$E_i = \frac{g_i N_{co_2} h\nu_i}{\exp\left(\frac{h\nu_i}{kT_i}\right)-1} \quad (i=1, 2, 3) \quad (1)$$

$$E_4 = \frac{N_{N_2} h\nu_4}{\exp\left(\frac{h\nu_4}{kT_4}\right)-1} \quad (2)$$

9

In the equations, N_{CO_2} and N_{N_2} represent, respectively, the numerical densities of CO_2 and N_2 molecules; $h\nu_1$, $h\nu_2$, and $h\nu_3$ represent, respectively, 1388 cm^{-1}, 667 cm^{-1}, and 2349 cm^{-1}; $h\nu_4$ is corresponding to 2331 cm^{-1}. The total energy of a unit gas is E.

$$E = \left(\frac{5}{2} N_{CO_2} + \frac{5}{2} N_{N_2} + \frac{3}{2} N_{He}\right) kT \quad (3)$$

In the equation, N_{He} is the numerical density of He gas. E_1, E_2, E_3, E_4, and E satisfy the following equations:

$$\frac{dE_1}{dt} = N_e(t) N_{CO_2} h\nu_1 z_1 - \frac{E_1 - E_1^*(T)}{\tau_{10}(T)}$$
$$- \frac{E_1 - E_1^*(T_3)}{\tau_{13}(T_3)} + \left(\frac{h\nu_1}{h\nu_3}\right)$$
$$\times \frac{E_3 - E_3^*(T, T_1, T_3)}{\tau_3(T, T_1, T_3)}$$
$$+ h\nu_1 \Delta NWI_0 \quad (4)$$

$$\frac{dE_2}{dt} = N_e(t) N_{CO_2} h\nu_2 z_2 + \frac{E_1 - E_1^*(T_3)}{\tau_{13}(T_3)}$$
$$- \frac{E_2 - E_2^*(T)}{\tau_{20}(T)} + \left(\frac{h\nu_2}{h\nu_3}\right)$$
$$\times \frac{E_3 - E_3^*(T, T_1, T_3)}{\tau_3(T, T_1, T_3)} \quad (5)$$

$$\frac{dE_3}{dt} = N_e(t) N_{CO_2} h\nu_3 z_3 - \frac{E_3 - E_3^*(T, T_1, T_3)}{\tau_3(T, T_1, T_3)}$$
$$+ \frac{E_4 - E_4^*(T_3)}{\tau_{43}(T)} - h\nu_3 \Delta NWI_\alpha \quad (6)$$

$$\frac{dE_4}{dt} = N_e(t) N_{N_2} h\nu_4 z_4 - \frac{E_4 - E_4^*(T_3)}{\tau_{43}(T)} \quad (7)$$

$$\frac{dE}{dt} = \frac{E_1 - E_1^*(T)}{\tau_{10}(T)} + \frac{E_2 - E_2^*(T)}{\tau_{20}(T)}$$
$$+ \left(1 - \frac{h\nu_2}{h\nu_3} - \frac{h\nu_1}{h\nu_3}\right)$$
$$\times \frac{E_3 - E_3^*(T, T_1, T_3)}{\tau_3(T, T_1, T_3)} \quad (8)$$

10

In the equations, $N_e(t)$ is the electron density and x_i is the electron excitation coefficient. $E_i^e(T_j)$ is the balancing values (i=1, 2, 4) of E_i at T_j; and $E_3^e(T, T_1, T_2)$ is the equilibrium value of E_3. τ_{10}, τ_{20}, τ_{12}, τ_{43}, and τ_3 are relaxation times between various energy levels; N is the difference in the particle populations between the upper and lower vibration energy levels of the laser; and W is the emission rate upon excitation at the center of the spectral lines (the above expression equation can refer to [3]). The intensity I_v in the cavity of the laser field satisfies the following equation:

$$\frac{dI_v}{dt} = -\frac{I_v}{\tau_v} - c\nu_L\lambda J_v NW I_v + W_e \quad (9)$$

In the equation, W_e is the item of spontaneous radiation, and ν is the laser frequency:

$$\tau_v = \frac{2L}{C}\left(\frac{1}{2\gamma L - \ln R_1 R_2}\right) \quad (10)$$

is the life span of laser cavity. In the equation, L is the laser cavity length: R_1 and R_2 are, respectively, the reflectivities of two terminal cavity vanes; generally, R_1=1 and R_2 is the reflectivity of the output vane, assuming $R=R_2$.

Equations (4) to (9) are one set of first-order differential equtions used in calculations.

LITERATURE

1. Beaulieu, J. A., Laser Focus, 6, No. 2 (1970), 14.

2. Cai Yingshi, Lou Chihong, and Ding Aizhen, Jiguang [Laser], 1979, 6, No. 2, 25.

3. Manes, K. R., and Seguin, H. J., J. Appl. Phys., 43 (1972), 5073.

4. Judd, O. P., J. Appl. Phys., 45 (1974), 4572.

5. Polanyi, J. C., Appl. Opt., Supplement on chemical laser (1965), 109.

6. Harrach, R. J., and Einwohner, T. H., USAEC UCRL-51399.

INVESTIGATIONS OF ULTRASHORT LASER PULSES--GENERATION, MEASUREMENT, SELECTION AND AMPLIFICATION

Tang Guisheng, Zhi Tingting, Xie Ziming, and Qiu Peixia
Shanghai Institute of Optics and Fine Mechanics, Chinese Academy of Sciences
Submitted 2 February 1979

Investigation results on ultrashort pulses of a passively mode-locked Nd glass laser are presented in this article. The generation, selection and amplification of the ultrashort pulses are described in particular. The effects of dye cell, dye concentration and the transmissivity of the output mirror on mode locking have been studied. The amplification factor and the signal-to-noise ratio for pulses of 10 ps to 130 ps have been measured. Some of the experimental results on interaction between ultrashort pulses and plasma are also included.

Abroad, a large numb - of studies were conducted on ultrashort pulses produced by passively mode-locked Nd glass lasers [1]. We have also studied ultrashort pulses for several years. One aspect of the studies is the production of picosecond pulses and nanosecond pulses in applied physics. The other aspect is seeking the mode-lock regime, to investigate the regime of saturated absorber mode-lock regime, to study effect of certain parameters on the mode-lock, and properties of ultrashort pulses.

12

I. Experimental Installation and Measuring and Test Methods

The experiments of mode-locked oscillators were conducted at two installations, such as (a) and (b) in Fig. 1. (a) shows a conventional oscillator and (b), a prototype used in laboratories. All these two installations are of semi-conjugate-foci cavity type, with cavity 1.5 meters in length; hence, one complete return-trip of light requires $T=2L/C=10$ nanoseconds. For a concave lens, the radius of curvature $R=3.0$ meters, and the output terminal is a wedge-shaped partial reflection mirror of 30' to 2°; the angle of the wedge-shaped plate is determined by the distance from the output cavity plate to the plane of rod terminal. In the installation (a), the rod dimensions are $\phi 12 \cdot 200$ (mm)$_{effective}$. The normal lines of two terminal planes and the optical axis form a small angle, by using a double-cylinder-shaped light-focusing cylinder to supply two straight-tube xenon lamps with a capacitance of 600 microfarads. The rod is cooled with water at constant temperature and these lamps are cooled naturally. In the sample device installation of Fig. 1(b), the cavity plate of the laser is placed on an Invar supporting frame; the entire laser is placed in an isothermal box and the temperature variation in the box can be controlled within 1°C. The terminal surface of the rod is ground into a Brewster's angle with dimensions as $\phi 10 \cdot 200$ (mm) and water cooling to maintain a constant temperature. The two straight-tube xenon lamps have dimensions of $\phi 10 \cdot 200$ (mm) with the matching of a double-ellipse light concentrating cylinder; these two lamps are connected in series with a capacitance of 150 microfarads. There is a dye box mounted on the sample device; the box and a concave (complete) reflection lens comprise an entity. This arrangement is helpful in eliminating the production of satellite pulses [2]. Moreover, selected-mode-of-transmission diaphragms with $\phi 2.5 \sim 3$ are placed in resonance oscillation cavities to ensure that the laser output is in the fundamental mode. A photograph of the fundamental-mode output field is shown in Fig. 2(a). After repeated demonstrations with several experiments, oscillation in the fundamental mode is among the necessary conditions for a good mode-locked laser.

The scanning and operating techniques of mode-locked pulses include the following:

13
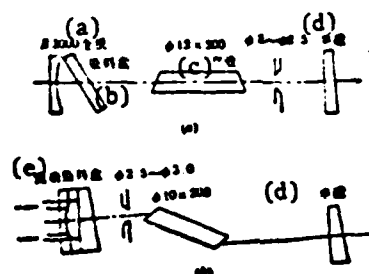
Fig. 1. Two types of mode-locked
Nd glass laser installations.
Key: (a) Total reflection; (b)
Dye box; (c) Effective; (d) Semi-
transmission; (e) Movable dye box.

(a) A photograph of the
output field in the
fundamental mode.

(b) A photograph of a mode-locked
pulse sequence.
Fig. 2.

(1) Energy: surveyed with highly sensitive calorimeter.

(2) Spatial distribution of energy: measurements calibrated photographically;
field-diagram sensitive paper is used for observation in ordinary experiments.

14

(3) Pulse sequence: observed with the Chinese-made high-current photoelectric tube GD-44.1 and a fast travelling wave 519 oscillograph [Fig. 7(b)].

(4) Pulse width and mode-lock quality: measured with the two-photon-fluorescence (TPF) method.

(5) Single-pulse--signal-to-noise ratio at back base: measured photoelectrically after amplification [5].

(6) Light extinction ratio of lithium niobate selection pulse switch: measured with energy method and photoelectric method [see II].

(7) Stability of mode-lock: closely observed with the waveforms, energy and TPF of oscillograph.

(8) Increment of ultrashort pulses: measured with the energy and power method [see II].

II. Explanations of Experiments and Results

1. Obtaining different pulse widths

By dissolving hendeca-methyl Sichuan [a province in China] blue into an acetone mode-lock; the thickness of liquid layer in the dye box is 1 mm, penetration rate at 60 percent, and the dye box is inserted into the cavity in the form of Brewster's angle. In this situation, 10 picoseconds pulses can be obtained; the photograph of TPF locus and the black density scanning locus can be referred to Fig. 3. In this arrangement, often satellite pulses appear beside the main pulses [as shown in (a) and (b) of Fig. 4]. The time difference between the main pulse and the satellite pulse is $\Delta T = 2\ell/C$; ℓ is the distance from dye box to the concave cavity plate.

The fluctuation regime or a saturated absorber mode-lock can explain the initiation cause of satellite pulses; the main pulses reflected from the cavity

15
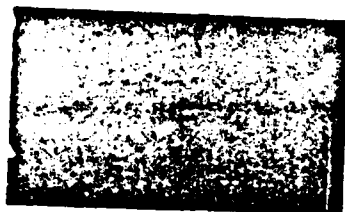
Fig. 3. TPF photograph of picosecond level pulses.

(a) 有明显卫星脉冲的微微秒脉冲 TPF 照片
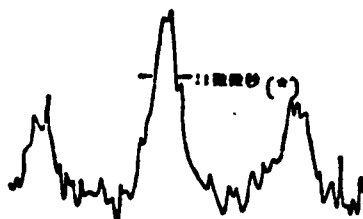
(b) 微微秒脉冲 TPF 黑密度扫描

Fig. 4: (a) TPF photograph of picosecond pulse with obvious satellite pulse; (b) TPF black density trace of picosecond pulse.
Key: (*) Picoseconds.

surface saturate the dye. At that time, a small pulse passes through the dye box at a reverse direction with no loss. Since the small pulse receives one less absorption loss, its net increment is greater. Therefore, the oscillation probability also increases.

16

If the dye box is so arranged that there is a small slope angle formed and close to a cavity plate or the dye box and concave lens become integrated, in both cases pulses of tens of picoseconds can be produced. Figure 5(a) shows a TPF photograph obtained with an integrated dye box (1 mm thick); 5(b) shows a photograph obtained when a standard tool (R=35 percent) coated at both sides with 0.32-mm thick membranes is placed in the cavity.

(a) 一体化染料盒的 TPF 黑片，$\tau_p \sim 25$ 微微秒

(b) 一体化染料盒腔内加 0.3 毫米($R=35\%$) 标准具的 TPF 黑片，$\tau_p=54$ 微微秒

Fig. 5: (a) TPF photograph of an integrated dye box, $\tau_p \sim 25$ picoseconds; (b) TPF photograph of an integrated dye box with addition of a piece of 0.3 mm (R=35 percent) standard tool.

If the dye box is constructed with a Brewster angle and a membrane-coated standard tool 0.5 mm thick, and the reflectivity of two surfaces is 20 percent, the output pulse width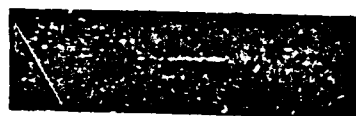 is approximately 80 picoseconds. By inserting three flat plates 0.2, 0.6 and 3.2 mm thick, the output pulse width is now approximately 130 picoseconds and the TPF photographs are shown in Figures 6 and 7. As indicated by experiments, if only a flat plate (or two plates) 0.2 or 0.6 mm thick is added, there is very small effect on pulse lengthening. The TPF photographs are shown in Fig. 8(a) and (b); i.e., the pulse width is little different in the case of without the standard tool.

2. Effect of dye concentration

As indicated in experiments, the dye penetrating rate increased from 50 percent to 70 percent, and the pulse widths went up from 24 picoseconds to 28

17
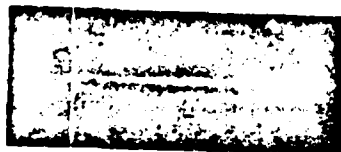
Fig. 6. TPF photograph--a piece of
0.5-mm thick standard tool (R=20
percent) is added in the cavity,
$\tau_p \sim 75$ picoseconds.

Fig. 7. TPF photograph--three pieces
of flat plates 0.2, 0.6 and 3.2-mm
thick are added in the cavity, $\tau_p \sim$
130 picoseconds.

picoseconds. As affected by unsteady pulses, they did not vary appreciably when
there is little variation of concentrations. This variation satisfies the mode-
lock principle of dyes. In other words, when the concentration is increased, the
threshold value of bleaching is increased and the pulse leading edges become
steep. Hence, the pulse width is correspondingly reduced.

The dye concentration affects not only pulse width, but also the probability
of occurrence of mode-locked pulses. As indicated by experiments, the mode-lock
is relatively stable under conditions of this experimental instalaltion and
within the range of 55 to 60 percent of dye penetration rates.

3. Effect of penetration rates of output cavity plate

18
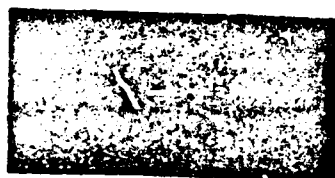
(a) 空内工一片 0.2 毫米的选模板的 TPF 照片

(b) 腔内工 0.2、0.6 毫米两块选模板的 TPF 照片

13皮秒

(*)
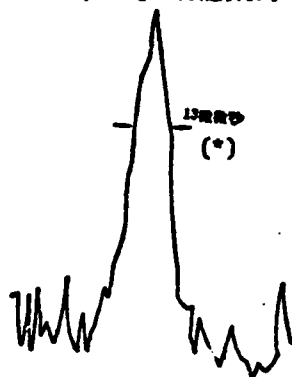
(c) 微微秒脉冲 TPF 黑密度扫迹（腔内加 0.2、
0.6 毫米平板标准具）

Fig. 8: (a) TPF photograph of adding a
piece of 0.2 mm thick selection mode plate
in the cavity; (b) TPF photograph of adding
two pieces of selection mode plates (0.2
and 0.6 mm thick) in the cavity; (c) TPF
black density trace of picosecond pulse
(adding two pieces of 0.2 and 0.6-mm thick
flat-plate standard tools).
Key: (*) Picoseconds.

The penetration rate of output cavity plate can affect intensity of mode-
locked pulses. When the penetration rate is relatively low, the two-photon-
fluorescence [TPF] is quite dark and even the illumination locus cannot be
recorded in photographs. Conversely, the TPF brightens. Very obviously, the

19

output power outside of the cavity intensifies because the penetration rate of the cavity plate is increased. Of course, the single-mode oscillation will be affected if the penetration rate is too high; if the number of high-order modes is too many, it is also disadvantageous to the locked mode. This explains the necessity of requiring a best matching.

In experiments, different penetration rates of T=70 percent, 50 percent, 45 percent, and 28 percent were adopted. As indicated by experiments, TPF is difficult to be photographed if T=28 percent. Usually, the penetration rate should be greater than 50 percent.

4. Selection of single pulses

The output of a mode-locked laser contains pulse sequences; one of the sequences can be selected if a pulse switch is used. Generally, a pulse switch consists of a KDP or KD*P crystal, deflection-initiating lens, deflection-examining lens, and laser-igniting spark gap. The adjustment of this type of switches is complex because there are many elements and large losses; the light extinction ratio is approximately of $10^{3[4]}$ or $10^{4[5]}$ in magnitude.

The authors selected a 45° single-piece lithium niobate and laser-igniting spark gap as a selection pulse switch. Figure 9 shows a schematic diagram of the selection pulse switch.

The output of mode-locked oscillator is a series of linear polarized mode-locked pulses; after the pulses pass through a polarized-light plate* located 90° outside of the cavity, the vibration direction of the electric field is perpendicular to the paper surface. When voltage is not applied to lithium niobate, the sequence pulses emit from a direction 0'. When a semi-wave potential is applied to lithium niobate as the voltage waves are instantaneously synchronized with the sequence pulses, then the selected pulses emit from e" direction. The authors used the laser-igniting spark gap as a potential

---

* The polarized-light plate is not essential. Adjustments are relatively complex without the plate. It is necessary to have a smaller angle for the crystal in order to modulate the e light [6].

instantaneous synchro switch; a half-wave potential rectangular pulse with width of approximately 9 nanoseconds is applied onto lithium niobate. Then only one pulse is ensured of selection and a relatively greater modulation depth exists.
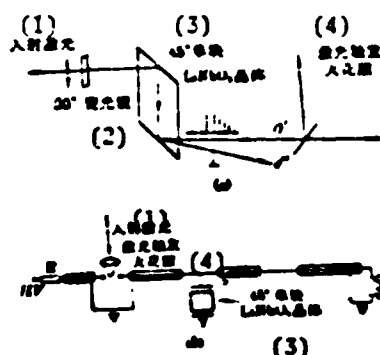
Fig. 9: (a) Schematic diagram of selection pulse switch; (b) Diagram showing connection of laser-igniting spark gap and LiNbO₃ crystal. Key: (1) Incident light; (2) Light polarizing lens; (3) 45° single piece of LiNbO₃ crystal; (4) Laser-igniting spark gap.

After the several parameters of spark sphere gap have been determined, single pulses are selected at different positions of sequence pulse. Table 1 lists the experimental parameters and results of selected pulses. Figure 10 shows a photograph of selected pulse.

The authors used the energy and photoelectric measurement methods. In the range of transmitted light values selected by the authors, the light extinction ratio of this piece of lithium niobate is measured as 1:3000. Whatever the method, it is carried out with the addition of two levels of a ∅20·500 mm rod-shaped amplifier.

The overall light extinction ratio of lithium niobate is relatively poor; however, if the diameter of laser-pulse light beam is small, in a transmitted light range with good local light quality, the light extinction ratio can be increased.

21

By using a 2-mm diameter helium-neon laser as a probing light beam, and examining the light extinction ratios of different crystals and different positions of the same crystal, it is known that there may be considerable differences in the light extinction ratios of various cuts of crystals and different positions of the same crystal cut; therefore, it is necessary to select and position in advance.

In short, the lithium niobate selected pulsed switch has the advantages of simple structure, convenient adjustment, and small loss. The light extinction ratio of a single cut of lighium niobate is 10^{-3} in magnitude. No breakdown of the laser occurs when the pulse power density is 10^8 to 10^9 watts.

5. Measurement of signal-to-noise ratio

According to the fluctuation theory of the saturable absorber passive locked mode [7], a certain back base will exist within the pulse intervals of the output sequence. The signal-to-noise ratio between mode-locked pulse and back base is one criterion in discriminating a good from bad locked mode. At the same time, the switching time of our selected pulse switch is approximately 10 nanoseconds. Within 10 nanoseconds, the single pulse and its back base simultaneously enter the amplifier level for amplification; amplification of the back base is injurious. Therefore, in the general experiment it is very necessery to know the magnitude of the signal-to-noise ratio in order to proceed with the overall design.

The authors adopted a method similar to Dobe's [8] in measuring the signal-to-noise ratio. Figure 11 is a measurement schematic diagram. An initiating signal is picked up from the inclined terminal plane of the third-stage amplifier to initiate the oscillograph for the high-current photoelectric tube P_1. The high-current photoelectric tube P_2 picks up the scanned signal from M_6 reflection mirror. The signals entering P_1 and P_2 delay relatively by 28 nanoseconds. With the amplification of three-level $\phi 20 \cdot 500$ mm Nd glass amplifier, the increment is greater than 10^{-3}. In the delayed light channel, an adequate attenuation vane S is placed so that the scanned signal has an adequate height to measure the distance x between starting points of the tracing and pulse signals. If after

22

Table 1. Experimental parameters and results of selected pulse switches.

(a) 半波电压	5200~6000 伏(o)	天 线(p)
	6500 伏(o)	理论(q)
调制深度(b)	14000~15400 伏(o)	<50%
(电源电压)	11000~11800 伏(o)	>75%
成形电缆 (c)	90 厘米(r)	
传输电缆 (d)	80 厘米(r)	
匹配电缆 (e)	50 米(s)	(防反射用)(t)
方波电压 (f)	~9 毫微秒宽(u)	
电极间距 (g)	0.4 毫米(v)	
球隙气压 (h)	12公斤/厘米²(w)	
充气气氛 (i)	75%	N₂
	25%	Ar
(j) 工作电压/自击穿电压	95%	
选出脉冲 (k)	1个(x)	
选出几率 (l)	>90%	
脉冲宽度 (m)	0.01~0.150 毫微秒(y)	
脉冲能量 (n)	~1 毫焦耳(z)	

Key: (a) Half-wave potential; (b) Modulation depth (source voltage); (c) Formed cable; (d) Transmission cable; (e) Matching cable; (f) Square-wave potential; (g) Distance between electrodes; (h) Gas pressure at sphere gap; (i) Pressure of gas filled; (j) Working potential/spontaneous puncturing potential; (k) Selected pulses; (l) Selected probability; (m) Pulse width; (n) Pulse energy; (o) Volts; (p) Experiments; (q) Theory; (r) cm; (s) Meters; (t) (Prevention of reflection); (u) About 9 nanoseconds wide; (v) mm; (w) kg/cm²; (x) Piece; (y) Nanoseconds; (z) Millijoule.

the back base intensity is amplified, the intensity exceeds the attenuation value of the attenuation vane, then no variation of x is seen. At that time, we only used a lithium niobate crystal cut as the element of the selected pulse switch with a light extinction ratio of 1:3000, then when the measured signal-to-noise ratio is greater than this value, the light-leaking pulse signal of lithium niobate switch element will be clearly shown.

23
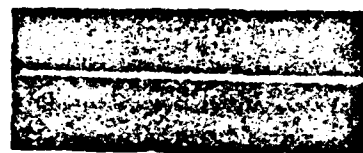
(a) 箭头指示的位置脉冲被选出
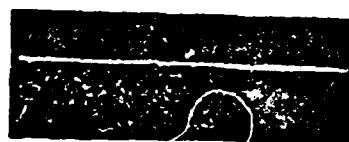
反冲干扰(*)

Fig. 10. Waveform of selection pulse:
(a) the pulse at the position pointed
by the arrow is selected; (b) the
selected single pulse as indicated by the
the arrow.
Key: (*) Anti-shock disturbance.
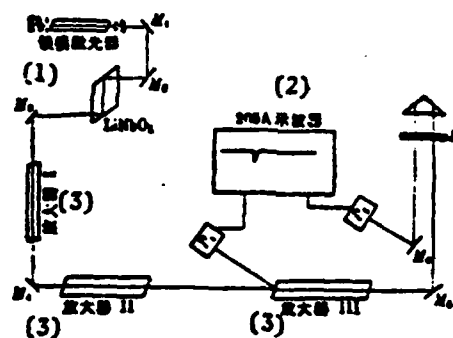
Fig. 11. Schematic diagram of experiments
of measuring the signal-to-noise ratio.
Key: (1) Mode-locked laser; (2) Oscillograph;
(3) Amplifier.

From the attenuatio: value and measuring distance x of the attenuation vane
S, the signal-to-noise ratio is known to be approximately 3000:1 for nanosecond
mode-locked pulse. The decrease in x is not discovered in the nanosecond range.

Since the combined response time of receiver and oscillograph is measured
in nanoseconds, the signal-to-noise ratio achieved lies outside the nanosecond
range. When this method is used, phenomena within the nanosecond range is not
understood; only by combining the scanning of contrast, the quality of locked
mode can be determined.

6. Amplification of nanosecond and picosecond pulses

As for the amplification of nanosecond (2 to 30 nanoseconds) pulses, there
are experiences. However, there is almost no experience with the amplification
of nanosecond pulses. However, the situation of amplifying nanosecond and
picosecond level pulses is very important to the design of a high power laser
system of this type of pulse width.

Fig. 12. Schematic diagram of experiment
of single pulse magnifier.
Key: (1) Mode-locked laser; (2) Amplifier;
(3) Funnel.

Researchers are concerned about whether the gain of nanosecond and picosecond
pulses differs considerably from the gain of nanosecond pulses. This is because
the nanosecond pulses mentioned by the authors have their output from a Pockels cell
[transliteration] box Q modulation Nd glass oscillograph and obtained by wave
clipping of two pockels photoelectric switches; the pulse width is approximately
2 nanoseconds and the spectrum width is approximately 50 Å. However, the nano-
second and picosecond pulses are required to have the output from the mode-locked

25

oscillograph limited by band width. Assuming that the spectrum and time are of the Gauss-type distribution, the full width at half-pole magnitude (HMFW) $\Delta\nu_{1/2}$ and $\Delta t_{1/2}$ should satisfy

$$\Delta\nu_{1/2}\Delta t_{1/2} = 0.44 \qquad (2)$$

If $\Delta t_{1/2} = 150$ picoseconds From equation (2), it is found that $\Delta\nu_{1/2} = 2.94 \cdot 10^9$ and the corresponding $\Delta\lambda_{1/2} = 0.11\text{Å}$. It can be seen that by comparing the sub-nanosecond pulses with the nanosecond pulses, it is an order of magnitude smaller in spectrum. smaller in time and three orders of magnitude Similarly, by comparing the sub-nanosecond pulses with nanosecond pulses, at least two orders of magnitude levels of difference in time exist. However, the gain of the laser amplifier is related to the band width and pulse width of output signals under the same conditions of light pump.

The authors used the sub-nanosecond pulses (pulse width approximately 130 picoseconds and energy of a single pulse approximately 1 millijoule) of output of Nd glass dye mode-locked oscillograph as sequence and single-pulse amplification. The picosecond pulse (pulse width approximately 10 picoseconds and the single-pulse energy approximately 1 millijoule) is amplified in single pulses. Figure 12 is the schematic diagram of the amplification experiment.

With the addition of the half-wave potential on lithium niobate, magnification of sequence pulse is obtained. The sequence amplification of sub-nanosecond pulses is measured in the first-stage amplifier. Figure 13 gives the gain increment curves of sequence amplification.

It can be seen from Fig. 13 that the number of amplifications of the sub-nanosecond and nanosecond pulses is already high, as many as 14 ∼ 20 times, and the number of amplifications of nanosecond pulses under the same optical pumping conditions does not differ much. We think that the possible reason these results were obtained is:

(1). The cross relaxation time of Nd glass is very fast, i.e. when the pulse is in the range of $10^{-10} \sim 1.0^{-11}$ seconds, can still in time allow replenishment of reverse particles.

(2) Were the nanosecond pulses amplified or not? Because the mode-lock pulse condition in the nanosecond range was not fully understood, there is a need for further research into mode-lock pulse conditions in the nanosecond range.

7. Some Overall Experimental Results.

Figure 14 is the schematic diagram of general experimental equipment. The general experimental equipment basically is a single-channel large device installation with 2 nanosecond pulse width. Only the mode-locked oscillograph and selected pulse system are used to substitute the original pockels cell Q modulation oscillograph and wave clipping system.
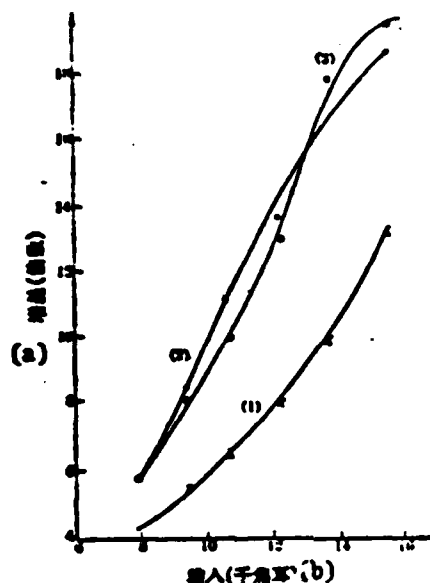
Fig. 13. Increment curves of sub-nanosecond and
picosecond pulses: (1) 7-72-21 rod, sub-nanosecond
sequence pulse; (2) 74-21 rod, sub-nanosecond single
pulse; (3) 74-21 rod, picosecond single pulse.
x sequence pulse of sub-nanosecond, • single pulse
of sub-nanosecond, and o single pulse of picosecond.
Key: (a) Increment (times); (b) Input (kilojoules).

The authors surveyed the increment of the fourth-stage amplifier. At
optimal delay time, when the input signal is 0.4 to 0.5 joule, the output is
approximately 5 joules and the increment is 10 times; the increment is not
much different from the original increment of a 2-nanosecond pulse gain.

Since the separation ratio (1:3000) of the lithium niobate selected pulse
switch is not high enough, between the third and the fourth levels, hendeca-
methyl Sichuan blue dye is used for separation to control light leakage and
super-radiation in order to conduct general target shooting experiments. Ten
picosecond and approximately 130 picosecond pulses, respectively, are used in

28

conducting experiments on shooting LiD plain target. When the 10 picosecond
pulse width is used, the general output is 15 joules and the electron tempera-
ture measured is 600 electron volts. When the approximately 130 picosecond
pulse width is used, the general output is 21 joules and the electron temperature
is measured as 700 electron volts. Operation of the device is normal; altogether,
20 replications of the target-shooting experiment were conducted with the device
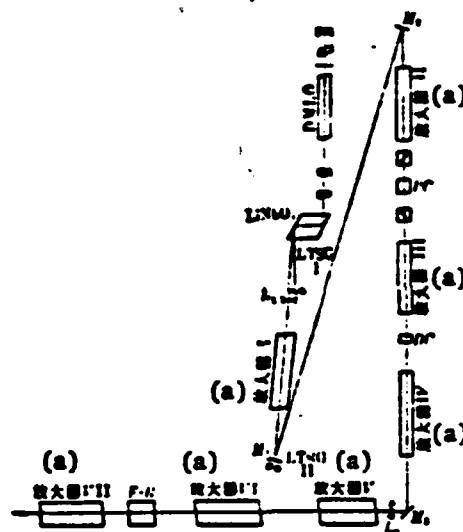operating normally.

Fig. 14. Schematic diagram of general experimental layout:
DMLO--dye mode-locked oscillograph; LiNbO$_3$--lithium niobate
selected pulse switch; LTSGI--laser-igniting spark gap used
for selected pulse; LTSGII--laser-igniting spark gap used
for Puke'er box; L$_1$--R=1 meter divergent lens; L$_2$--R=10
meters convergent lens; PC--Puke'er cutoff switch; F-R--
faraday separator; M$_1$, M$_2$, M$_3$--plain reflection mirrors;
amplifier I amplifier; IV--ϕ20·520 mm; amplifier V--ϕ35·520 mm;
amplifier VI, VII--ϕ40·520 mm; DC--dye box.
Key: (a) Amplifier.

III.   Stability of Mode-locked Oscillograph

The re-emergence characteristics of the saturable absorber passive locked
mode are poor. The main manifestations are as follows: the envelope of mode-locked

pulse sequence of each shooting differs, and even two- or multiple-row pulses appear. During each shooting, there are different widths for each pulse in the pulse sequence. The pulse energy is different in each shooting; there is a difference in pulse smoothness, and even the appearance of sub-structures.

The results of a set of experiments conducted on an experimental passive mode-locked laser prototype device are listed in Table 2. Altogether, 12 experiments were continuously conducted; nine times with good pulse sequence waveforms and the others with two-row or fish-belly-shaped waveforms. From the table, for undesirable waveforms, energy values are on the high side; for good waveforms, the energy variation is ±10 percent. The pulse widths can be divided into two categories; one type is about 25 picoseconds with 7 times, and the other type, about 39 picoseconds. Within each type, the variation in pulse width from one type to another is of the skip type, which may be related to the linear spectrum structure. The variation of linear spectrum cannot be continuous. Thus, the variation in pulse width also cannot be of the continuous variation type. In the table, the contrast K of TPF is a reference value, which is at the higher side because the error of measurement is relatively high.

Table 2. Data of mode-locked pulses of a set of continuous shooting.

次序 No. (a)	TPF·对比 度 K (b)	脉宽 τ$_p$ (微微秒) (c)	脉冲平列 能量(格) (d)	示波器波 形记录 (e)
1	2.88	25.4	19	好 (f)
2	2.9	28.8	20	好 (f)
3	3.5	39	22	好 (f)
4	3.6	23.7	26	双列 (g)
5	3.08	25.4	18	好 (f)
6	2.82	23.7	19	好 (f)
7	2.95	39	36	好 (f)
8	3.08	40.9	29	双列 (g)
9	2.88	22	21	好 (f)
10	2.90	37.2	20	好 (f)
11	—	37.2	26	好 (f)
12	2.88	25.4	27.5	双列 (g)

Key: (a) Sequence no. (b) Contrast K of TPF;
(c) Pulse width τ$_p$ (picoseconds); (d) Pulse
sequence energy P(lattice); (e) Waveform
recording of oscillograph; (f) Good; (g) Two
rows.

The stability of the passive locked mode is determined by the regime of the dye locked mode. The passive mode-locked pulse originates in noise; the increment of the passive system of pulse-type operation is entirely exhausted in noise; the increment of the passive system of pulse-type operation is entirely exhausted even before the pulses are operated in a steady state. Therefore, the final mode-locked pulse must also include noise properties. It the statistical rule has not been completely avoided, it is impossible to have good re-emergence. Generally, it is considered that the appearance of good-mode-locked probability is related to the relaxation time of the saturated absorber. If the pulse is longer than the dye relaxation time, the stability is relatively good. Conversely, the stability is relatively poor. However, this is different in the case of the steady-state locked mode [9, 10]. Hence, the achievement of steady-state locked mode is the fundamental way of improving stability.

Next, the thermal effect of dye solution is also one very important parameter [11] of achieving mode-locked stability. Since the several interactions of laser and dye will gradually deteriorate the dye, affecting the locked mode, therefore flowing dye should be a necessary condition for ensuring a steady locked mode. For our devices with 6 to 10 operations, the dye flows to another box; however, there is no strict boundary.

In order to maintain the output stability as far as possible, the following points should be taken into account in the experiments: the first is to avoid harmful feedback inside or outside of the cavity; the second is that the dye penetration rate of each experiment should be the same; the third is that the time interval should be controlled between the various shootings to allow laser to have certain thermal stability conditions; and the fourth is to carefully control the light pump input with operation near the threshold value.

LITERATURE

[1] R. C. Greenhow, A. J. Schmidt; Advances in Quant. Electr., 2, part2 (1974).
[2] P. W. Smith, M. A. Duguay, E. Q. Ippen; Progress in Quant. Electr., 3, part2.
[3] G. Dube; Appl. Phys. Lett., 18, 69 (1971).
[4] D. V. D. Linde, O. Bernecker, W. Kaiser; Opt. Commun., 2, 149 (1970).
[5] I. Souras et al.; Appl. Opt., 13, No. 9, 230 (1974).

[6]   Jiguang [Laser], 1975, 2 No. 2, 8 to 19.

[7]   W. H. Glenn; *IEEE J. Quant. Electr.*, QE-11,
      No. 1, 8—17 (1975).
[8]   G. Duba; *Appl. Phys. Lett.*, 18, 69 (1971).
[9]   D. V. D. Linde; *IEEE J. Quant. Electr.*, QE-8,
      No. 3, 728 (1972).
[10] D. J. Kuizenga; *Opt. Commun.*, 22, No. 2, 156—
      160 (1977).
[11] R. Wilbrandt, H. Weber; *IEEE J. Quant.
      Electr.*, QE-11, No. 5, 186 (1975).

END

FILMED

8